Journal of Power Sources 196 (2011) 1163–1170

Contents lists available at ScienceDirect

Journal of Power Sources

journal homepage: www.elsevier.com/locate/jpowsour

A comparison of high-speed flywheels, batteries, and ultracapacitors on the bases of cost and fuel economy as the energy storage system in a fuel cell based hybrid electric vehicle

Reed T. Doucette*, Malcolm D. McCulloch

Department of Engineering Science, University of Oxford, Thom Building, Parks Road, Oxford, OX1 3PJ, United Kingdom

ARTICLE INFO

Article history:
Received 9 June 2010
Received in revised form 19 July 2010
Accepted 29 August 2010
Available online 6 September 2010

Keywords:
Flywheel
Ultracapacitor
Battery
Hybrid
Electric
Vehicle

ABSTRACT

Fuel cells aboard hybrid electric vehicles (HEVs) are often hybridized with an energy storage system (ESS). Batteries and ultracapacitors are the most common technologies used in ESSs aboard HEVs. High-speed flywheels are an emerging technology with traits that have the potential to make them competitive with more established battery and ultracapacitor technologies in certain vehicular applications. This study compares high-speed flywheels, ultracapacitors, and batteries functioning as the ESS in a fuel cell based HEV on the bases of cost and fuel economy. In this study, computer models were built to simulate the powertrain of a fuel cell based HEV where high-speed flywheels, batteries, and ultracapacitors of a range of sizes were used as the ESS. A simulated vehicle with a powertrain using each of these technologies was run over two different drive cycles in order to see how the different ESSs performed under different driving patterns. The results showed that when cost and fuel economy were both considered, high-speed flywheels were competitive with batteries and ultracapacitors.

1. Introduction

High-speed flywheels are an emerging technology with characteristics that have the potential to make them viable energy storage systems (ESSs) aboard vehicles. This paper investigates the competitiveness of high-speed flywheels on the bases of cost and fuel economy when compared to the more well established energy storage technologies of batteries and ultracapacitors in a fuel cell based series hybrid electric vehicle (HEV).

Amidst growing concerns over energy security, climate change, air pollution, and fossil fuel reserves, alternatives to conventional automobile powertrains based on internal combustion engines (ICEs) are being investigated [1,2]. Powertrains based on fuel cells are one such alternative that have the potential to overcome many of the problems endemic to ICEs [3,4]. Fuel cells typically have a higher "tank to wheel" efficiency than ICEs, and depending on how the hydrogen fuel is generated they have the potential to emit significantly fewer pollutants [5].

Hybridizing a fuel cell with an ESS can have several positive impacts [6]. The ESS can be designed to meet the transient power demands that characterize normal driving conditions. With the ESS handling the transient loads, the fuel cell only has to provide the average power [2]. This enables the fuel cell to be downsized which reduces costs and typically improves efficiency [7]. The ESS provides the additional benefit of being able to store energy captured through regenerative braking [2].

Most of the work done in designing and optimizing series HEVs has only considered batteries and/or ultracapacitors as the ESS [2,8–11]. While previous research has produced a great deal of information about optimal ESS technologies and configurations, it has largely neglected high-speed flywheels as an ESS technology that could compete with ultracapacitors and batteries.

Flywheels are a mature energy storage technology, but in the past, weight and volume considerations have limited their application as vehicular ESSs [12]. The energy, E, stored in a flywheel is expressed by

$$E = \frac{1}{2} J\omega^2 \quad (1)$$

where J is the inertia and ω is the angular velocity. From Eq. (1), it can be seen that greater energy gains come from increasing the speed of a flywheel than from increasing the inertia. Improvements in low friction bearings and high tensile strength and low density materials have now made high speeds attainable hence making lightweight flywheels a reality [13]. For instance, the flywheel used in this study weighs 15 kg (including packaging), has a maximum speed of 60,000 rpm, and is capable of storing 540 kJ [14–16]. The Ragone plot in Fig. 1 shows that flywheels achieve specific energy

* Corresponding author. Tel.: +44 (0) 7769715340; fax: +44 (0) 1865273010.
E-mail addresses: reed.doucette@gmail.com (R.T. Doucette), malcolm.mcculloch@eng.ox.ac.uk (M.D. McCulloch).

0378-7753/$ – see front matter © 2010 Elsevier B.V. All rights reserved.
doi:10.1016/j.jpowsour.2010.08.100

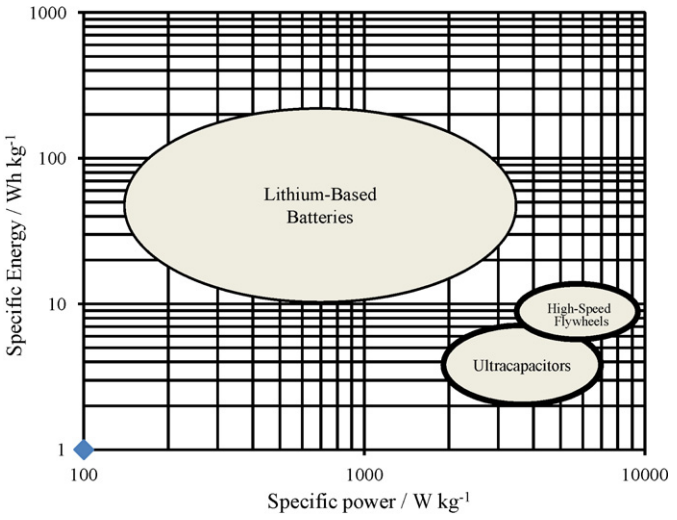

Fig. 1. Ragone plot of the different ESS technologies considered in this study.

and power ratings that should make them competitive with existing ESS technologies [14–20].

High-speed flywheels also have several unique charging properties. Flywheels, as well as ultracapacitors, have the benefit over batteries of a high cycle life with little decrease in efficiency [21]. Due to their high specific power, flywheels, along with ultracapacitors, can charge and discharge much quicker than batteries. The most crucial performance drawback of high-speed flywheels is that they experience relatively high losses which cause them to self-discharge more rapidly compared to batteries and ultracapacitors [22,23]. For instance, the high-speed flywheel used in this study will go from fully charged to fully discharged in around 15 min with no other forces acting on it aside from its internal losses.

Prior studies have examined the modeling and implementation of flywheel systems in vehicles [12,24,25]. However, previous research has not provided a direct comparison between high-speed flywheels, ultracapacitors, and batteries functioning as the ESS in an HEV. This study aims to make that comparison. In this study, computer models of those three different ESS technologies were developed and integrated into a vehicle simulation program written in MATLAB. Simulations were run over a range of different ESS configurations utilizing different control strategies over two drive cycles. The performance of the three different technologies was then evaluated for their effect on fuel economy and cost.

2. Models

2.1. Vehicle simulator

The vehicle simulator used in this study is called OVEM (Oxford VEhicle Model) [26]. It was developed by the author to allow for novel simulation of electric and hybrid electric vehicle powertrains. OVEM uses a backwards–forwards simulation similar to ADVISOR [27]. This simulation method was used because it achieves reliable results with quick run-times, and it is also able to incorporate models based on readily available data [28].

A backwards–forwards simulation begins by calculating the torque and speed that a vehicle must produce in order to meet a given drive cycle based on the sum of the following forces [29]: aerodynamic drag,

$$F_D = \frac{1}{2}\rho C_D A_f v^2 \tag{2}$$

rolling resistance,

$$F_{RR} = \mu_{RR} mg \tag{3}$$

and acceleration

$$F_A = ma \tag{4}$$

where C_D is the drag coefficient, A_f is the frontal area of the vehicle, v is the linear speed of the vehicle, μ_{RR} is the rolling resistance coefficient, m is the mass of the vehicle, g is the acceleration due to gravity, ρ is the density of air, and a is the acceleration of the vehicle. Once the torque and speed that the vehicle must produce to meet the drive cycle have been calculated, the torque and speed requests proceed through the powertrain with each component factoring in its own losses and imposing its physical limits.

In the series HEV model used in this study, a representation of which can be seen in Fig. 2, the wheel/axle block receives the initial torque and speed requests and accounts for its own losses. In this study, the wheel/axle bearing losses were assumed to be fixed at 1% of the transmitted power, and that was held constant for all the ESS types. The wheel/axle block then passes a revised torque and speed request which factors in its power losses to the gearbox block. The gearbox block in this study calculates its efficiency based on

$$\eta = \frac{T_{in}\omega_{in}}{T_{in}\omega_{in} + k_{\text{seal}} N^2 T_{\text{max motor}}\,\omega_{in} + (k_{\text{mesh}} + k_{\text{bearing}}) T_{in}\omega_{in}} \tag{5}$$

where T_{in} and ω_{in} are the torque and speed respectively received from the wheel/axle block, N is the gear ratio (which in this study was set to 2), and $T_{\text{max motor}}$ is the maximum torque of the motor [30]. The dimensionless gearbox coefficients are empirically derived and remain constant throughout the simulation. The coefficient of the losses due to the seals, k_{seal}, was set to 0.00103, k_{mesh} accounts for the gear meshing losses and was set to 0.02, and k_{bearing} accounts for the bearing losses and was set to 0.005 [30]. The gearbox block accounts for its losses and applies the gear ratio before passing on a revised torque and speed request to the motor and power electronics block. The efficiency of the motor and power electronics is represented by an efficiency map where efficiency is plotted as a function of torque and speed [31]. The motor and power electronics block incorporates its losses into the power request it sends to the electric bus. The power request on the electric bus is satisfied by the ESS and fuel cell to the best of their ability given their power rating and the state of charge (SOC) of the ESS. The power capable of being supplied by the ESS and fuel cell is passed to the electric bus to prepare to move forward through the blocks. The

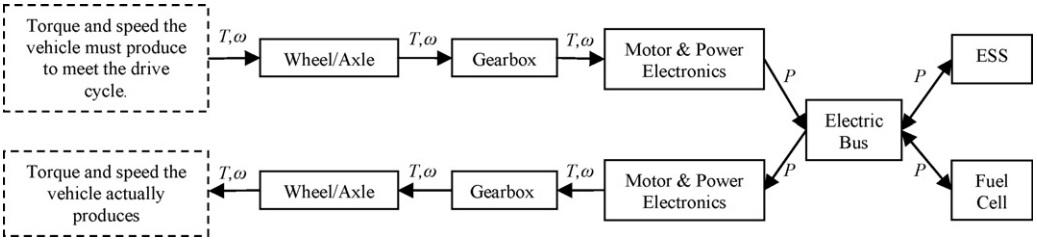

Fig. 2. Information flows in the OVEM series HEV model.

motor and power electronics block receives the power delivered on the electric bus and computes the amount of torque and speed it can produce based on the amount of power it receives. In instances where the amount of power the motor block receives is less than the power it requested, the motor produces torque such that the ratio between torque and power is the same as was requested during the backwards phase of the simulation. The torque and speed signals continue to move forward through the gearbox and wheel/axle blocks with each accounting for their losses until the model outputs the torque and speed achieved by the vehicle over each one second time step in the drive cycle.

The OVEM model requires that the drag coefficient, frontal area, rolling resistance coefficient, tire radius, glider mass (curb weight excluding the mass of the ESS, fuel cell, and motor) be specified. In order to obtain these parameters, the author conducted a survey of popular mid-size sedans in the United States for which this data was provided by the manufacturers: 2008 Toyota Camry Solara, 2009 BMW 525, 2008 Mercedes C-Class, 2007 Nissan Altima, 2008 Mazda 6, and 2009 Volkswagen Passat. The average of each of the specifications was ultimately used in this investigation which resulted in the simulated vehicle having a drag coefficient of 0.29, a frontal area of 2.2 m^2, a tire radius of 25 cm, and a glider mass of 1250 kg. The coefficient of rolling resistance was set to 0.01 and the density of air was set to 1.2 kg m^{-3} [29].

2.2. Fuel cell model

Since this study was only concerned with the overall electrical characteristics and fuel consumption of the fuel cell, the fuel cell model in this study utilized the power–current (*P–I*) and efficiency curves published for fuel cells of different power ratings. A survey of published data for PEM fuel cells agreed with Bauman and Kazerani [9] which showed that it was reasonable to assume that the shape of the *P–I* and efficiency curves for cells of any power rating were similar when the power and current axes were scaled by their maximum values, P_{max} and I_{max} [6,32–35]. The *P–I* and efficiency curves used by the model were the average of the scaled curves from an array of commercially available fuel cells with different power ratings. Figs. 3 and 4 show the data obtained from the fuel cells and the average curves used in the model for the *P–I* and efficiency curves respectively.

The survey of commercially available fuel cells also revealed that the relationship between the mass and the power rating of a fuel cell can be reasonably represented by a power law relationship as seen in Fig. 5. Thus, the fuel cell model only requires that the maximum power of the fuel cell be specified, and from that the fuel cell mass, *P–I* curve, and efficiency curve can all be determined. When the fuel cell model receives a power request, it determines the mass of the hydrogen that must be consumed in order for it to meet that power request based on the lower heating value of hydrogen, 120 MJ kg^{-1}. There is a wide range of estimates for fuel cell cost as they involve approximations about the cost reductions that fuel cell manufacturing will experience with increased production. With high-volume production, Tsuchiya and Kobayashi and Jeong and Oh [36,37] estimate that PEM fuel cells will cost between $200 and $400 per kilowatt. This was the cost range used in this study, making fuel cells the most expensive power source in the vehicle.

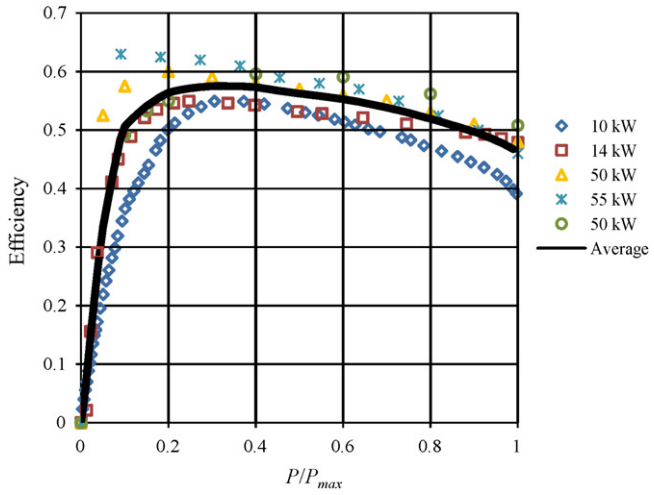

Fig. 4. Normalized efficiency curves for an array of commercially available fuel cells [6,32–35].

2.3. Flywheel model

The flywheel model is based on data for a 540 kJ, 60 kW flywheel from Flybrid Systems [14–16]. In the model, the flywheel handles requests to produce or accept a certain amount of power to the maximum extent permitted by its current SOC and power rating. The flywheel's losses are accounted for through a lookup table that relates the power losses to the speed of the flywheel [15]. The losses in a given time step were found by taking the average speed of the flywheel over that time step and then finding the corresponding power loss. It should also be made explicitly clear that not all spec-

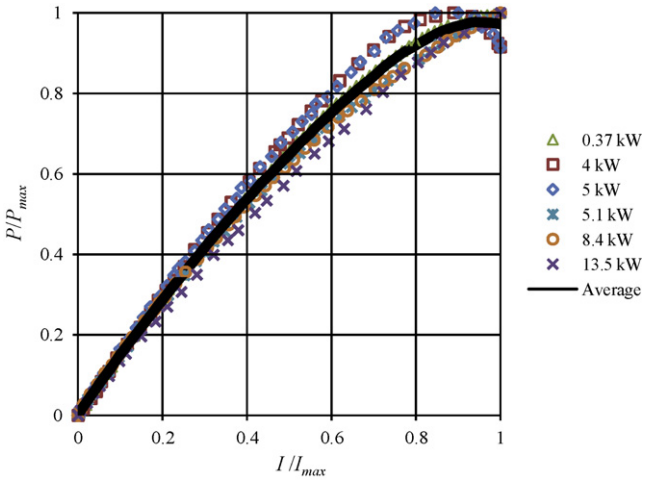

Fig. 3. Normalized *P–I* curves for an array of commercially available fuel cells [6,32–35].

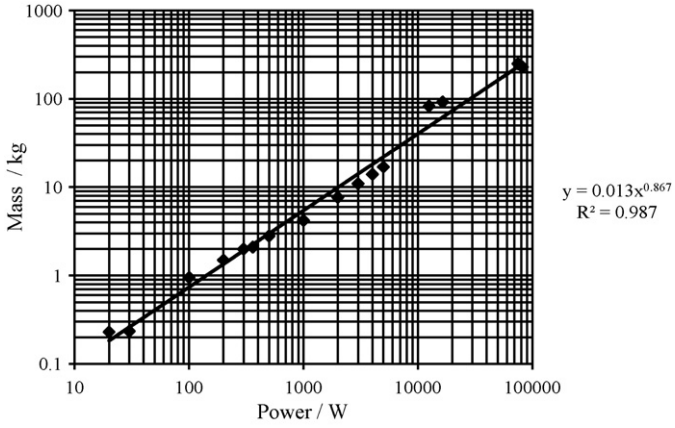

Fig. 5. Relationship between mass and maximum power of an array of commercially available PEM fuel cells [6,32–35].

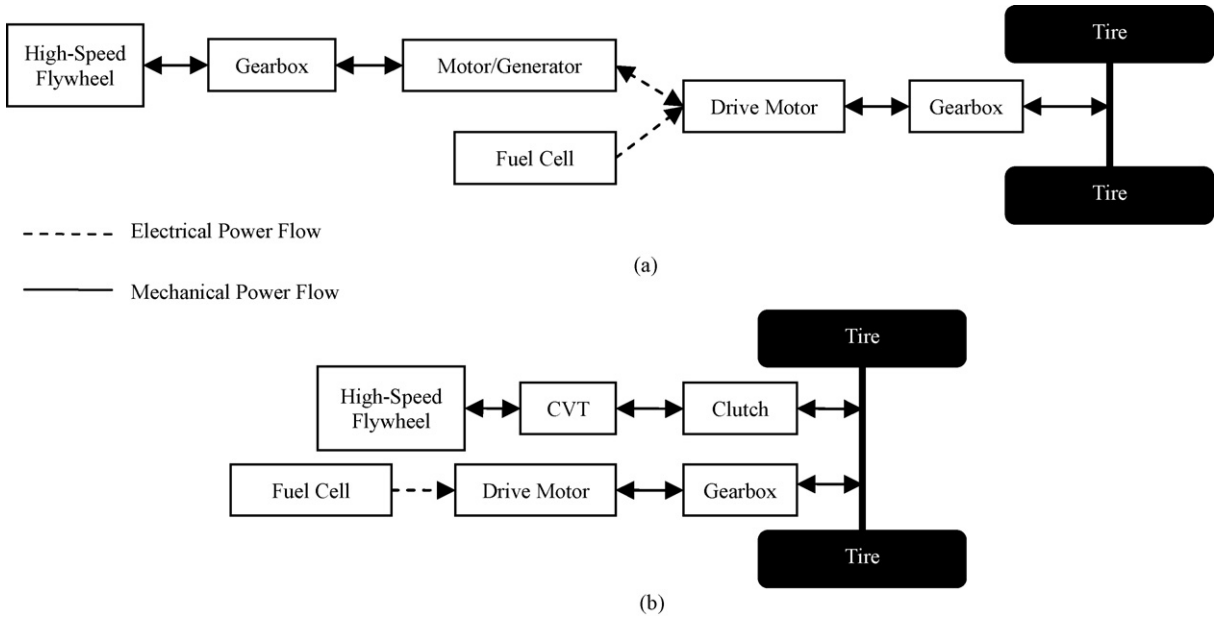

Fig. 6. (a) Electrically integrated high-speed flywheel connected to the electric bus through a motor/generator. (b) Mechanically integrated high-speed flywheel connected to the drive axle via a CVT.

ifications for this flywheel are yet publically available, and certain data required for this study were obtained through a personal correspondence with Flybrid Systems. As imperfect as this may be, Flybrid Systems is, to the best of the author's knowledge, the only manufacturer of mechanically integrated, high-speed flywheels for automotive applications. Therefore in order to proceed with this analysis, their data was used.

A flywheel functioning as an ESS is generally integrated into a powertrain in one of two ways as seen in Fig. 6 [38]. In the first method, known as electrical integration, the flywheel is connected, usually through a fixed ratio gearbox, to an electric motor/generator which is connected to the electric bus. This method allows for more flexibility in packaging the flywheel system in the vehicle. In the second method, known as mechanical integration, the flywheel is connected to a continuously variable transmission (CVT) which interfaces with the driveshaft via a clutch. Integrating the flywheel via the CVT is more efficient, since the flywheel does not receive power that has been subjected to motor/generator, gearbox, and wheel/axle losses. For this reason, a mechanically integrated high-speed flywheel was used in the study. Prior research has shown the efficiency of the CVT is approximately 85% regardless of the power passing through it [14]. Therefore in this study the CVT model was treated as having a fixed efficiency of 85%.

Proper packaging for high-speed flywheels is critically important so that the device is contained in the event of a rupture. The combined mass of the standard flywheel (including its packaging) used in this study is 15 kg. Through correspondence with a Flybrid representative, it was estimated that with high-volume production a CVT for a 60 kW flywheel would weigh approximately 48 kg. According to Flybrid's cost estimates based on mainstream automotive market production volume, the standard flywheel should cost between $1000 and $3000 and the CVT should cost no more than $1500 which brings the total flywheel system cost to between $2500 and $4500 or $42–$75 per kilowatt.

Though the standard flywheel used in this study weighs 15 kg and stores 540 kJ, the flywheel size can be varied. It was determined that the mass of the flywheel rotor could be decreased by 20%, however the mass of the flywheel system cannot be increased because the 15 kg version is the largest flywheel that the bearings in this study could handle [15]. If more energy storage is required from the flywheel, then multiple flywheels must be used. If multiple flywheels are used together, the mass, energy storage, cost, and losses are increased by a factor equal to how many flywheels are connected together and added to the fixed cost and mass of the ancillary flywheel equipment. If the mass of the flywheel is reduced by 20%, the cost and mass scale linearly yet the power losses remain the same because the same bearings are used as in the standard flywheel.

2.4. Ultracapacitor model

The ultracapacitor model in this study is based on a 350 F ultracapacitor [20]. The model treats the ultracapacitor as a voltage source, E, in series with an ideal resistor, R, which represents the internal resistance of the device, and V_{terminal} is the voltage measured at the terminals of the ultracapacitor as seen in Fig. 7.

The open-circuit voltage of the ultracapacitor as a function of the SOC is defined by a lookup table published by the manufacturer as seen in Fig. 8 [39]. The resistor has a constant value and is set to the value reported as the internal resistance in the device's datasheet, 3.2 mΩ. This ultracapacitor has a specific energy of 5.62 Wh kg^{-1} and a specific power of 4.3 kW kg^{-1} [20]. The literature quotes ultracapacitors as costing between $0.01 and $0.015 per Farad in high-volume production [40]. This puts the cost between $3.50 and $14 per cell and between $13 and $51 per kilowatt.

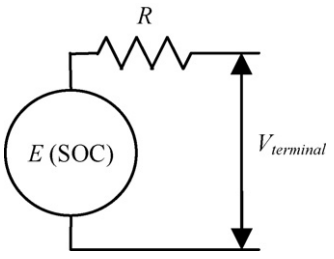

Fig. 7. Diagram of the equivalent circuit for the ultracapacitor and battery models.

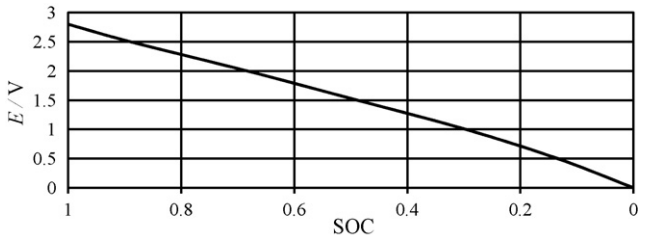

Fig. 8. The open-circuit voltage of the 350 F ultracapacitor as a function of its SOC.

2.5. Battery model

The batteries used in this study were used because they are commercially available lithium-ion cells that are marketed by their manufacturer for use in HEVs [41,42]. Lithium-ion batteries were used in this study because their specific energy and power ratings are amongst the highest of all battery technologies. The cells in this study have a specific energy of 108 Wh kg^{-1} and a specific power of 3.3 kW kg^{-1} [42]. The model treats the battery as a voltage source in series with a resistor similar to the ultracapacitor model as seen in Fig. 7 [9]. Just as with the ultracapacitor model, E varies with the SOC and R is constant. However, the method for determining E and R for the battery model differs from the method used for the ultracapacitor model. In order to obtain E and R, the battery model uses the procedure outlined in [43,44] which require data that can be obtained from the constant current discharge curves on the battery's datasheet. Fig. 9 shows the agreement between the data provided by the battery's datasheet (points labeled "exp") and the predictions for E based on the model (line labeled "sim") for a range of discharge currents. The battery manufacturer has published a cost of $110 per 6 cells ($2400 kWh^{-1}) though this price is only quoted for small shipments intended for experimental use, and it is considerably higher than most cost estimates for lithium-based batteries in 2010. A more reasonable cost estimate was obtained that put the cost of the batteries at between $1000 and $2000 per kilowatt-hour, or between $33 and $66 per kilowatt, and this was the figure used in this study [45].

2.6. Drive cycles

The fuel economy of a vehicle is affected to a large degree by the drive cycle over which it is tested. So in order to more completely

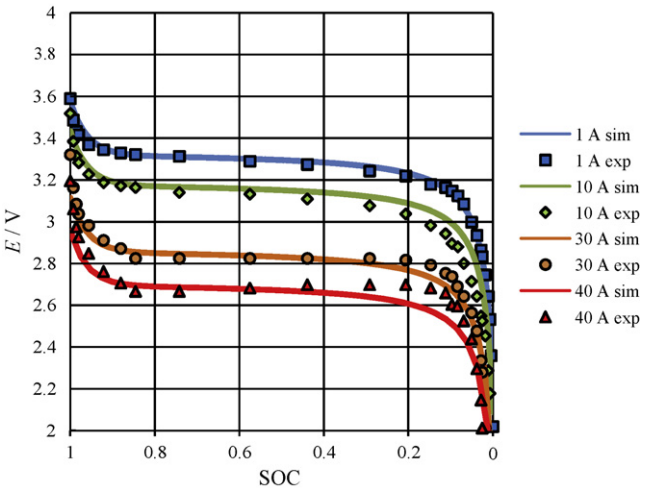

Fig. 9. The model's prediction compared to the manufacturer supplied data for the open-circuit voltage as a function of SOC for a range of discharge currents for the lithium batteries used in this study.

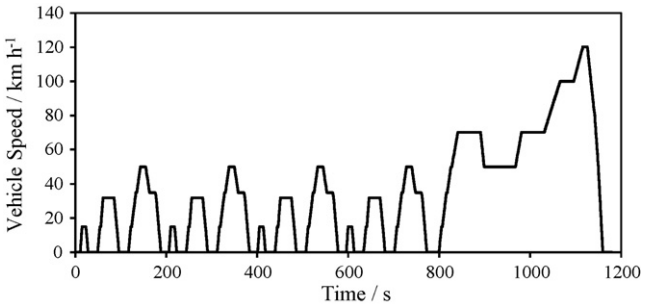

Fig. 10. New European Drive Cycle.

characterize a given powertrain, it must be examined over different drive cycles. In this study, the vehicle was tested over 12 iterations (82.1 miles) of the New European Drive Cycle, seen in Fig. 10, and 4 iterations (83.5 miles) of the Artemis Combined Drive Cycle (ACDC), seen in Fig. 11. The number of iterations was selected so that the vehicle would travel close to the same distance over both of the drive cycles. The NEDC was chosen because it is the basis for emissions testing in Europe. The ACDC places the motorway Artemis drive cycle immediately following the urban Artemis drive cycle. The ACDC was chosen because it is a more aggressive drive cycle with both a demanding urban and highway component that is more representative of real world driving [46].

3. Control strategies

The control strategy selected for an HEV can have a dramatic impact on its performance [6]. Previous studies have examined optimal strategies for fuel cell series HEVs that do not know the drive cycle in advance [6,47]. Those studies form the basis for the control strategy used for the battery and ultracapacitor. However due to the lack of literature on control strategies for mechanically integrated high-speed flywheels, one was devised by the author for this study.

3.1. Flywheel

In this study, the flywheel only recharges through regenerative braking. It would be possible for the flywheel to receive excess power generated by the fuel cell so that it could recharge in the absence of a braking event to prepare for a future acceleration event. However, this pathway is inefficient, and charging the flywheel exclusively through braking was shown in the initial work of this investigation to be a more efficient control strategy. Thus, it was the strategy employed in this study.

During a motoring event (acceleration or constant speed driving), the controller first requests the power from the flywheel and the flywheel supplies as much power as it can in an effort to meet that request. If the flywheel is unable to fully meet that request

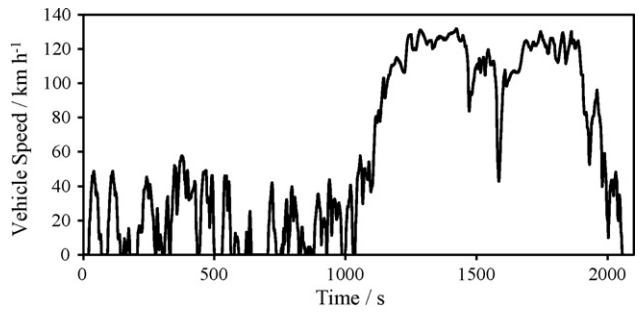

Fig. 11. Artemis Combined Drive Cycle.

on its own then the controller turns to the fuel cell to provide the remaining power. Once the flywheel is fully discharged, the fuel cell must meet all of the power requests until the flywheel's SOC increases via energy captured through regenerative braking.

3.2. Ultracapacitor and battery

Like the flywheel, the ultracapacitor and battery modules receive energy from regenerative braking and provide energy during acceleration and constant speed motoring. Yet unlike the flywheel, they are able to receive power from the fuel cell with lower losses. Hence the efficiency of the powertrain can be improved by recharging the ultracapacitors and batteries with excess power generated by the fuel cell.

The control strategy used in this study was based on the work of Schiffer et al. [6] which showed that the SOC of the ESS should be kept inversely proportional to the vehicle's speed. This strategy is based on the premise that at low speeds it is likely that the vehicle will accelerate in the near future, and the ESS should have a high SOC so that it can power that acceleration. At high speeds, it is likely that the vehicle will be braking soon so the ESS should have a low SOC which will allow it to accept as much of the regenerative braking energy as possible. Whenever the inequality below was true, the fuel cell was called upon to provide extra power to recharge the ESS

$$(1 - \mathrm{SOC}) > \frac{v_{\mathrm{current}}}{v_{\mathrm{max}}} \tag{6}$$

where v_{current} refers to the current speed of the vehicle and v_{max} refers to the vehicle speed at or above which the fuel cell no longer needs to produce power to recharge the ESS. In this study, the best fuel economy was achieved when v_{max} was set to 80 km h^{-1}, so that was the v_{max} used throughout the simulations. When the fuel cell was called upon to recharge the ESS, it did so at its point of optimal efficiency which was at 31% of the rated power as seen in Fig. 4.

4. Simulation results and discussion

4.1. Fuel cell sizing

As the most expensive power source in the powertrain, the power rating of the fuel cell was kept as low as possible to minimize overall powertrain costs. In this study, the goal was to keep the agreement between the velocity requested by the drive cycle and the velocity achieved by the vehicle to be within 2% and to never exceed 3 km h^{-1}. Given that constraint, the fuel cell size varied between 29 and 45 kW for the range of ESS technologies and sizes.

4.2. Flywheel, ultracapacitor, battery comparison

The cost of the batteries and ultracapacitors is directly proportional to their number and mass. As an additional cell is added to the array, the cost and mass of the array both increase by the amount of that one cell. The flywheel was examined at its standard specifications (15 kg and 540 kJ), with a 20% reduction in energy storage and mass, and with two and three standard flywheels connected together.

Figs. 12 and 13 plot the fuel economy of the vehicle (measured in kilometers per kilogram of hydrogen gas consumed) against the cost of the ESS (in US Dollars) for the three different ESS technologies. Figs. 14 and 15 plot the fuel economy of the vehicle against the total power source cost (ESS plus fuel cell). The ideal ESS would be as close to the top left corner of Figs. 12–15 as possible as this would represent an ESS that minimizes costs and maximizes fuel economy.

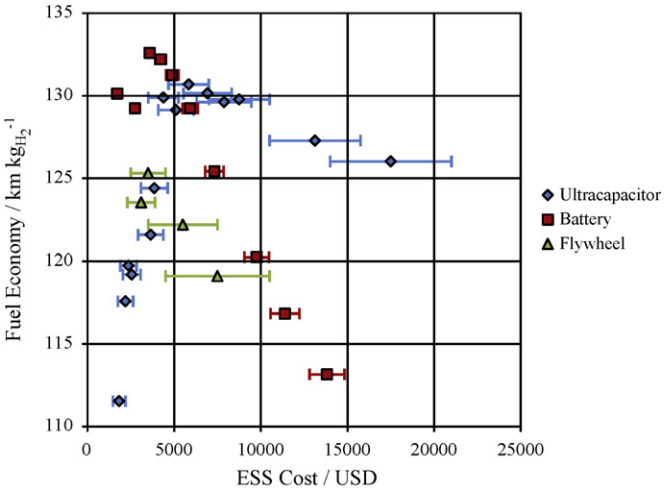

Fig. 12. Fuel economy as a function of ESS cost on the NEDC.

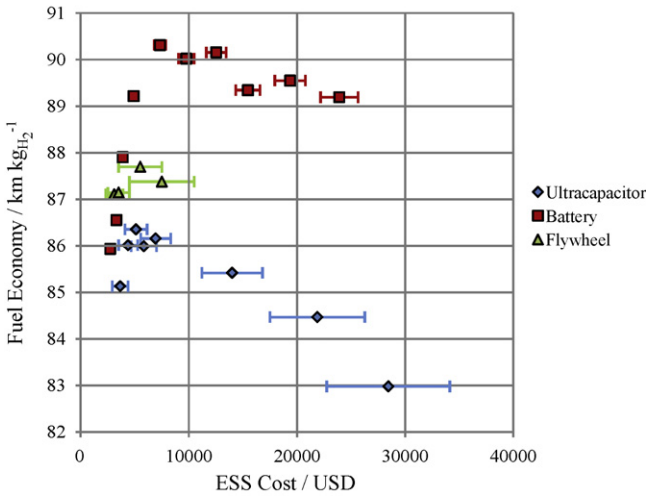

Fig. 13. Fuel economy as a function of ESS cost on the ACDC.

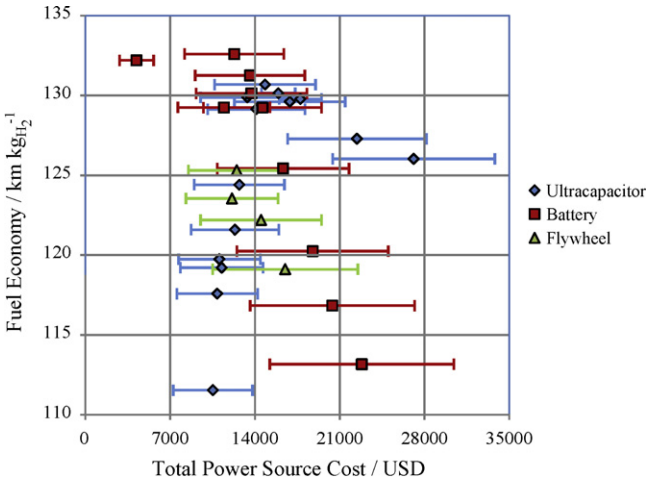

Fig. 14. Fuel economy as a function of total power source (fuel cell + ESS) cost on the NEDC.

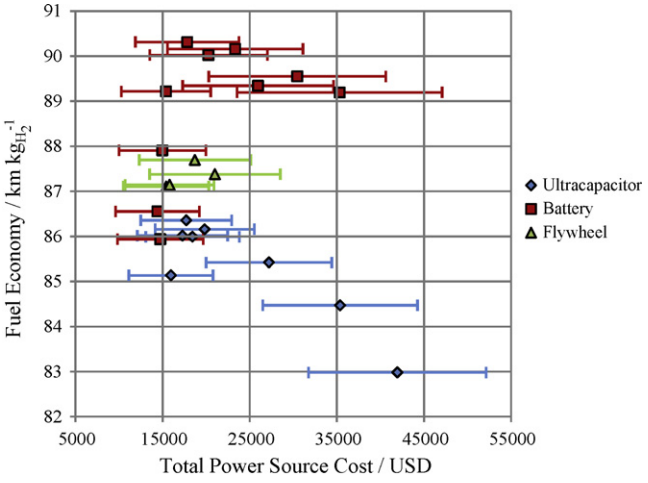

Fig. 15. Fuel economy as a function of total power source (fuel cell + ESS) cost on the ACDC.

On the NEDC, the fuel economy of the most fuel efficient flywheel (standard size) was 4% and 6% lower than the most fuel efficient ultracapacitor and battery arrays respectively. The most fuel efficient flywheel costs approximately the same as the most fuel efficient battery array, and is potentially up to 2.8 times less expensive than the most fuel efficient ultracapacitor array. Battery arrays costing less than the most fuel efficient flywheel achieve approximately 4% higher fuel economy. Ultracapacitor arrays costing approximately the same as the most fuel efficient flywheel achieve between 3% higher to 7% lower fuel economy.

On the ACDC, the most fuel efficient flywheel configuration occurs when two flywheels are connected together. The most fuel efficient battery array achieves 3% higher fuel economy than the most fuel efficient flywheel and roughly 4% higher fuel economy than the standard flywheel, though both of these flywheel combinations have the potential to be less expensive than the most fuel efficient battery array. The most fuel efficient flywheel achieves a fuel economy within 1% of similarly priced battery arrays. Every flywheel configuration achieved a higher fuel economy than the most fuel efficient ultracapacitor array on the ACDC, and the most efficient flywheel cost approximately the same as the most efficient ultracapacitor array.

Once the cost of the fuel cell is accounted for as seen in Figs. 14 and 15, the differences in cost of the powertrains employing the different ESS technologies were significantly reduced. This is due to the high cost of the fuel cells (and the large uncertainty in their cost) relative to the cost of the ESS. The small differences in cost between the different ESS technologies become overshadowed by the fuel cell costs.

5. Conclusion

This paper provides a comparison between high-speed flywheels (mechanically integrated into the powertrain via a CVT), ultracapacitors, and lithium-ion batteries serving as the ESS in a series HEV with a fuel cell. The three different technologies were compared through a vehicle simulation program, and the data used for the ESSs in the simulation all came from commercially available products. Each of the three technologies was simulated over a range of sizes. The results from this study showed that a vehicle with a high-speed flywheel as an ESS never achieved the highest fuel economy of the three ESSs tested on either drive cycle. Yet on the New European Drive Cycle, the fuel economy of the most efficient high-speed flywheel was only 4% and 6% lower than the most fuel efficient ultracapacitor and battery arrays respectively, and the high-speed flywheel had the potential to offer cost savings. On the Artemis Combined Drive Cycle, the flywheel achieved a higher fuel economy than any of the ultracapacitor arrays simulated and achieved approximately the same fuel economy as similarly priced battery arrays. These results show that in future studies high-speed flywheels should be considered as alternatives to ultracapacitors and batteries in fuel cell series HEVs.

Future work could benefit from reducing the uncertainty in the costs of the various components, especially in the fuel cells. In this study, it was shown that once the cost of the fuel cells was accounted for along with the ESS cost, many of the comparatively small differences in ESS costs were eclipsed by the relatively large fuel cell costs. It should be mentioned that these costs do not reflect the lifetime costs of any of these ESS components. It is likely that ESS technologies with higher cycle lives (such as flywheels and ultracapacitors) will be less expensive over the course of the vehicle's lifetime. Future research efforts should seek to better understand those life cycle costs.

References

[1] V. Mehta, J.S. Cooper, J. Power Sources 114 (2003) 32–53.
[2] P. Thounthong, S. Raël, B. Davat, J. Power Sources 193 (2009) 376–385.
[3] G. Cacciola, V. Antonucci, S. Freni, J. Power Sources 100 (2001) 67–79.
[4] A. Burke, Proc. IEEE 95 (2007) 806–820.
[5] L Carrette, K.A. Friedrich, U. Stimming, ChemPhysChem 1 (2000) 162–193.
[6] J. Schiffer, O. Bohlen, R.W. De Doncker, D.U. Sauer, K.Y. Ahn, Proc. IEEE Veh. Power Propuls. Conf (2005) 341–348.
[7] W. Gao, IEEE Trans. Veh. Technol. 54 (2005) 846–855.
[8] M. Uzunoglu, M.S. Alam, Energy Convers. Manage. 48 (2007) 1544–1553.
[9] J. Bauman, M. Kazerani, IEEE Trans. Veh. Technol. 57 (2008) 760–769.
[10] R.M. Schupbach, J.C. Balda, M. Zolot, B. Kramer, Power Electronics Specialist Conference, 2003. PESC '03. 2003 IEEE 34th Annual, vol. 1, 2003, pp. 88–93.
[11] G. Pede, A. Iacobazzi, S. Passerini, A. Bobbio, G. Botto, J. Power Sources 125 (2004) 280–291.
[12] O. Briat, J.M. Vinassa, W. Lajnef, S. Azzopardi, E. Woirgard, IET Electr. Power Appl. 1 (2007) 665–674.
[13] R. de Andrade Jr., et al., Proc. Int. Conf. Mater. Mech. Supercond. 408–410 (2004) 930–931.
[14] D. Cross, C. Brockbank, SAE World Congress and Exhibition, 2009.
[15] Personal Correspondence with Flybrid Systems (2009).
[16] Flybrid Systems, Available: www.flybridsystems.com.
[17] P.J. Hall, E.J. Bain, Energy Policy 36 (2008) 4352–4355.
[18] F.V. Conte, Elektrotecknik und Informationstechnik 123 (2006) 424–431.
[19] Maxwell Technologies, K2 Series Ultracapacitors Datasheet, 2010. Available: www.maxwell.com.
[20] Maxwell Technologies, BC Energy Series Radial D Cell 350 F Ultracapacitor Datasheet, 2010. Available: www.maxwell.com.
[21] Y. Gao, S.E. Gay, M. Ehsani, R.F. Thelen, R.E. Hebner, Veh. Technol. Conf., 2003. VTC 2003-Fall. 2003 IEEE 58th, vol. 5, 2003, pp. 3321–3325.
[22] J.W. Kimball, B.T. Kuhn, R.S. Balog, IEEE Trans. Power Electron. 24 (2009) 952–962.
[23] A. Burke, J. Power Sources 91 (2000) 37–50.
[24] H. Liu, J. Jiang, Energy Build. 39 (2007) 599–604.
[25] P.P. Acarnley, et al., IEEE Trans. Ind. Appl. 32 (1996) 1402–1408.
[26] R.T. Doucette, The Oxford Vehicle Model Manual: a Tool for Modeling and Simulating the Powertrains of Electric and Hybrid Electric Vehicles, University of Oxford, Department of Engineering Science, 2010. Available: http://epg.eng.ox.ac.uk/?q=node/44.
[27] K.B. Wipke, M.R. Cuddy, S.D. Burch, IEEE Trans. Veh. Technol. 48 (1999) 1751–1761.
[28] T. Markel, et al., J. Power Sources 110 (2002) 255–266.
[29] M. Ehsani, Y. Gao, S.E. Gay, A. Emadi, Modern Electric, Hybrid Electric, and Fuel Cell Vehicles: Fundamentals, Theory and Design, CRC Press, New York, 2005.
[30] T.J. Woolmer, The YASA Machine: For High Performance Automotive Applications, University of Oxford, DPhil Thesis, 2009.
[31] UQM Technologies, PowerPhase 150 Traction System Datasheet, 2009. Available: www.uqm.com.
[32] Hydrogenics, Hydrogenics HyPM Fuel Cell Power Modules Datasheet, 2009. Available: www.hydrogenics.com.
[33] Horizon Fuel Cell Technologies, H-Series PEM Fuel Cell Systems Datasheet, 2010. Available: http://horizonfuelcell.com/fuel_cell_stacks.htm.
[34] Nedstack, Datasheet for Nedstack P5 Fuel Cells, 2007. Available: www.nedstack.com.
[35] Schunk Group, Manual for Schunk Fuel Cell Stacks, 2008. Available: www.schunk-group.com.
[36] H. Tsuchiya, O. Kobayashi, Int. J. Hydrogen Energy 29 (2004) 985–990.
[37] K.S. Jeong, B.S. Oh, J. Power Sources 105 (2002) 58–65.
[38] J. Van Mierlo, P. Van den Bossche, G. Maggetto, J. Power Sources 128 (2004) 76–89.

[39] J.M. Miller, D. Nebrigic, M. Everett, Ultracapacitor Distributed Model Equivalent Circuit for Power Electronic Circuit Simulation, Maxwell Technologies Inc., 2006, Available: www.ansoft.com.
[40] A. Burke, EET-2007 European Ele-Drive Conf., 2007.
[41] S.B. Peterson, J. Apt, J.F. Whitacre, J. Power Sources 195 (2010) 2385–2392.
[42] A123 Systems, High Power Lithium Ion ANR26650 M1A Datasheet, 2009, Available: www.a123systems.com.
[43] C.M. Shepherd, J. Electrochem. Soc. 112 (1965) 657–664.
[44] O. Tremblay, L.A. Dessaint, A.I. Dekkiche, IEEE Veh. Power Propuls. Conf. (2007) 284–289.
[45] BERR & DfT, Proceedings of the Reform, 2008.
[46] M. Andre, Real-world driving cycles for measuring cars pollutant emissions – part a: The artemis European driving cycles, Laboratory Transport and Environment, Bron, France, nLTE 0411, 2004.
[47] S. Barsali, C. Miulli, A. Possenti, IEEE Trans. Energy Convers. 19 (2004) 187–195.